PCCP

PAPER

Cite this: *Phys. Chem. Chem. Phys.*, 2023, **25**, 21595

Phase coexistence in $[C_{22}/C_1MIm]^+[NO_3]^-$ ionic-liquid mixtures and first-order phase transitions from homogeneous liquid to smectic B by varying the cation ratio

Jie Yao,[ab] Giacomo Saielli,[cd] Fanlong Meng[abe] and Yanting Wang *[abe]

We perform molecular dynamics simulations to investigate the transition processes of $[C_{22}/C_1MIm]^+[NO_3]^-$ binary mixtures by varying the cation ratio of C_{22} to C_1 at a fixed temperature of 400 K. The cation ratio is tuned by ranging C_{22} percentage from 0% to 100% with a fixed number of 4096 total simulated ion pairs. Our simulated-annealing results indicate that, at 400 K, pure C_1 is a homogeneous liquid whilst pure C_{22} is an ionic liquid crystal (ILC) of smectic-B (SmB) type. With increasing C_{22} percentage, the system goes through a first-order phase transition from homogeneous liquid to nano-fragment liquid in the range from 15% to 17.5%, during which some of the individual cationic alkyl side chains locally aggregate to form small bundles "floating" in the polar "solvent" composed of anions and cationic head groups. Although the side chains in each bundle are parallelly aligned, the bundles distribute randomly without a global orientation. As the C_{22} percentage further increases, another first-order phase transition occurs to bring the system into the SmB ILC phase. Particularly, when the C_{22} percentage is in the range from 45% to 50%, the SmB phase coexists with the liquid phase containing both individual and bundled alkyl side chains.

Received 12th April 2023,
Accepted 22nd July 2023

DOI: 10.1039/d3cp01670f

rsc.li/pccp

Introduction

Ionic liquids (ILs) are molten salts at room temperature that have attracted much attention from both experimentalists and theorists on account of their extensive applications in industries.[1] For nearly two decades, various novel properties of ILs have been revealed, which greatly help the applications of ILs in many fields, such as green solvents,[2] catalysts,[3] solar cells,[4] membranes,[5] and conductivity materials.[6,7] ILs are composed of pure ions, for example, cations of imidazolium, ammonium, and pyridinium, while $[NO_3]^-$, $[BF_4]^-$, $[PF_6]^-$, and halides are commonly used anions. One of the vital traits of ILs is the formation of the nanoscale segregation liquid (NSL) phase[8–10] caused by the dual ionic and organic nature of ions[11] with both hydrophobic and hydrophilic moieties: when the alkyl cationic side-chain length is intermediate, the hydrophilic moieties form a continuous polar network enveloping the hydrophobic parts into it, resulting in microscopic spatial heterogeneity. Many works[12–14] have been devoted to investigating the transition of ILs between the NSL and ionic liquid crystal (ILC), namely, the liquid crystal phase formed by ILs. The stability of an IL is determined by the competition between the contributions to free energy from hydrophobic and hydrophilic parts, respectively, and can be tuned by varying anion species, the length of the cationic alkyl chain, temperature, *etc.*, to induce phase transitions from the NSL to ILC.[12,15,16] The desired structure of ILs can also be obtained by picking out an appropriate combination of cations and anions.[17] In practice, ILs composed of multiple types of ions can extend the ability of finely tuning their physicochemical properties like density, viscosity, ionic conductivity, dielectric permittivity, and melting point.[18,19] In particular, we are interested in what will happen if the concentration of long alkyl cationic side chains is tuned by mixing long-chain and short-chain cations with different ratios.

Recently, by molecular dynamics (MD) simulation, it has been found that increasing the cation ratio of 1-dodecyl-3-methylimidazolium bis(trifluoromethanesulfonyl)imide (abbreviated as C_{12}) to 1,3-dimethylimidazolium bis(trifluoromethanesulfonyl)imide (abbreviated as C_1) in the $[C_{12}/C_1MIm]^+[Tf_2N]^-$

[a] *CAS Key Laboratory of Theoretical Physics, Institute of Theoretical Physics, Chinese Academy of Sciences, 55 East Zhongguancun Road, P. O. Box 2735, Beijing, 100190, China. E-mail: wangyt@itp.ac.cn*
[b] *School of Physical Sciences, University of Chinese Academy of Sciences, 19A Yuquan Road, Beijing, 100049, China*
[c] *CNR Institute on Membrane Technology, Unit of Padova, Via Marzolo, 1 – 35131, Padova, Italy*
[d] *Department of Chemical Sciences, University of Padova, Via Marzolo, 1 – 35131, Padova, Italy*
[e] *Center for Theoretical Interdisciplinary Sciences, Wenzhou Institute, University of Chinese Academy of Sciences, 1 Jinlian Road, Wenzhou, 325001, China*

mixture promotes the emergence of the NSL phase from the homogeneous liquid phase,[20] which qualitatively explains previous experimental results for the same IL mixture.[21] Now we want to further ask, if the alkyl side chain is so long that the pure long-chain IL exhibits the ILC phase, how does the short-chain/long-chain IL mixture transform from a homogeneous liquid to ILC when varying the cation ratio?

As a background for comparison, we first briefly review the traditional liquid crystal (LC) theory. The most common LC phases formed by rod-like molecules are isotropic, nematic, and smectic. After the Maier–Saupe model[22–24] manifesting that the phase transition from isotropic to nematic is first order, by extending it to include the smectic phase, McMillan[25] showed that the transition from isotropic to smectic directly is also first order, while the transition from smectic to nematic is either first order or continuous[26] depending on temperature and external field. A great deal of works have then delved into extending these theories to the studies of LC polymers,[27,28] LC microemulsion,[28] colloidal LCs,[29] and ILCs.[30] However, some of these systems are so different from traditional LCs that the existing theories cannot perfectly explain their phase behaviors. In the case of ILCs, for example, microphase segregation between ionic and alkylic components is the main driving force, so very few systems are capable of forming the nematic phase except for those whose ions are attached with rigid anisotropic cores,[31,32] and the stability of the nematic phase formed by ILs can be enhanced by increasing the anisotropy of rigid molecules.[33,34]

In this work, by MD simulation with the effective-force coarse-grained (EF-CG) model at a fixed temperature of 400 K,[35,36] we study the IL mixture of $[C_{22}/C_1MIm]^+[NO_3]^-$, in which $[C_1MIm]^+$ (abbreviated as C_1) is mixed with $[C_{22}MIm]^+$ (abbreviated as C_{22}), and they share the same kind of anion $[NO_3]^-$. The IL system with pure C_1, analogous to inorganic molten salts, exhibits the homogeneous liquid state, while that with pure C_{22} is capable of forming ILC in a broad temperature range due to the amphiphilic feature of C_{22}.[12,13,37,38] Our simulation results discover that two first-order phase transitions occur from homogeneous liquid (pure C_1) to smectic B (SmB) ILC (pure C_{22}) when varying the cation ratio. With a fixed number of total ion pairs, as the C_{22} percentage is in the range from 5% to 12.5%, the alkyl side chains of C_{22} distribute separately and individually in the polar "solvent" composed of $[NO_3]^-$ along with the imidazolium head groups of both C_1 and C_{22}. Starting at about 15%, the system goes through a first-order phase transition, after which some of the C_{22} side chains aggregate locally to form small bundles "floating" in the polar "solvent", referred to as the nano-fragment liquid (NFL). In the NFL phase, the nonpolar chains in each bundle are parallelly aligned to each other, rather than being pushed by the continuous polar network into huddles as in the NSL phase,[5,6,39] but the bundles are randomly distributed without a global orientation. The second first-order phase transition from the NFL to the SmB ILC occurs in the range of 45%–50%. In the SmB ILC, the side chains between charged layers are hexagonally packed, but retain their fluidity mainly due to the ions dispersed in the charged layers. In particular, during this phase transition, the homogeneous liquid, NFL, and SmB phases coexist in the system composed of individual, bundled, and layered side chains of C_{22}. At a higher C_{22} ratio, almost all of the C_{22} side chains self-assemble into SmB with very few distributed individually.

It is well known that ILs rarely form nematic ILCs, a result attributed to their isotropic cores of most kinds and flexible side chains.[33,40] Comparing our simulation results for the IL mixtures with traditional LC theories, we can see that, during the second first-order phase transition, alkyl side chains retain bundles until the structure of the polar parts changes from a polar network to separate layers. As a result, by increasing the C_{22} percentage, the IL mixture goes through a phase transition directly from isotropic to smectic without going through the nematic phase.

Methods

Simulation settings

By employing the EF-CG force field,[35] we carried out MD simulations for $[C_{22}/C_1MIm]^+[NO_3]^-$ mixtures with the C_{22} percentage ranging from 0% to 100%. We first scanned the phase behaviours with a coarse interval of 10%, and then used a finer interval of 2.5%, or even smaller when necessary, to better pinpoint the phase transition points. The total number of ion pairs is kept at 4096, so varying the C_{22} percentage is equivalent to tuning the cation ratio of C_{22} to C_1.

The EF-CG model along with the atomistic molecular structures of the simulated ILs is shown in Fig. 1, where the cationic head ring is coarse-grained to be CG site A, the single methyl group bonded with A is B, the four charged methylene groups on the long side-chains near A are sequentially M1, M2, M3, and M4, and the rest of the uncharged methylene groups are all grouped into CG sites C except the terminal methyl group, which is denoted as CG site E. The anion $[NO_3]^-$ is coarse-grained as CG site D. Further details of the EF-CG force field for the ILs and its parameters can be found in ref. 36.

All MD simulations were carried out in the constant *NPT* ensemble with the GROMACS 5.1.4 software package.[41] To allow the system to form an ILC structure, the pressures in

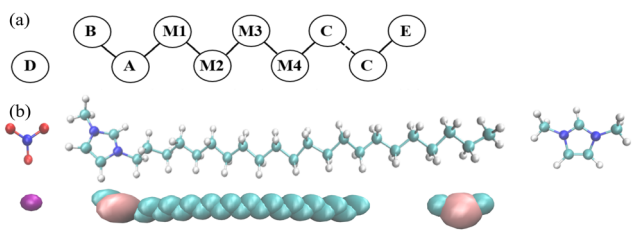

Fig. 1 (a) Coarse-grained model of C_{22}. (b) Atomistic molecular structure (upper) compared with the coarse-grained structure (lower) of the anion (left), C_{22} (middle) and C_1 (right). For the atomistic structure, the red spheres represent oxygen atoms, blue nitrogen, cyan carbon, and white hydrogen. For the coarse-grained structure, the violet sphere represents CG site D, pink CG site A, and cyan carbon groups.

the three dimensions vary independently, controlled by the Parrinello–Rahman barostat[42] at P = 1 bar in each dimension. The Berendsen barostat[43] was only employed at very high temperatures to maintain the stability of the simulation procedure. As a result of the anisotropic pressure, the simulation box is parallelepiped. The periodic boundary condition (PBC) is applied in all three dimensions and the time step is 4 fs. The simulation temperature is kept at T = 400 K by the Nosé–Hoover thermostat.[44] Both of the van der Waals (VDW) and the Coulomb interactions in the real space have a cutoff of 1.4 nm, and the Particle-mesh Ewald method[45] is adopted to deal with the long-range part of the Coulomb interaction.

The initial configurations were obtained by careful simulated-annealing procedures as follows. We first manually constructed the lattice structure of C_{22} in a very large box and inserted other small ions randomly, followed by equilibrating these systems by the isotropic Parrinello–Rahman barostat for about 1 ns at P = 100 bar and T = 10 K. The lattice structure was then completely relaxed by increasing the temperature to T = 2000 K with a constant pressure of P = 1 bar followed by applying a high pressure of P = 100 bar at T = 1200 K to press it from gas back to liquid, and the Berendsen barostat was only employed during this process. The system was then annealed from 1200 K to 700 K at P = 1 bar, being cooled down step by step with a temperature interval of 100 K, and running for 4–8 ns at each temperature. Subsequently, the systems were simulated sequentially at T = 600, 500, and 400 K with an anisotropic barostat. At each temperature, the equilibrating simulation time was ranged from tens to one hundred nanoseconds until the potential curve was completely converged, followed by a sampling run of 10 ns to evenly sample 2500 configurations at T = 400 K.

Data analysis

The most apparent feature of a first-order phase transition is the latent heat, which usually appears to be a kink in the potential energy curve of a given system when varying a certain thermodynamic variable. However, in this study, when varying the cation ratio, the IL mixtures we simulate have different total molecular weights, so the kinked feature is submerged in the molecular difference. Hence it is necessary to modify the original potential energy data to signify the kink(s), if any. The system potential energy U can be divided into self and interaction parts:

$$\langle U(c)\rangle = N(1 - c)\langle u_1\rangle + Nc\langle u_2\rangle + \varepsilon \quad (1)$$

where c is the C_{22} percentage, N = 4096 is the total number of ion pairs, $\langle u_1\rangle$ and $\langle u_2\rangle$ represent the mean potential energies of each C_1 and C_{22}, respectively, presumed to be constants when they lie in the same phase at a fixed temperature, and ε represents the interaction potential energy between ions. Therefore, there should have a partial potential energy that depends linearly on the C_{22} percentage.

Based on the linearity of the potential energy with respect to the C_{22} percentage, we define the relative potential energy U_r to evaluate whether there is a first-order phase transition or not. By subtracting the linear part at each percentage, the remaining energy U_r is obtained by

$$U_r(c) = \langle U(c)\rangle - \xi c - U_0 \quad (2)$$

The slope ξ can be obtained by fitting $\langle U(c)\rangle$ linearly depending on c before the first phase transition, and U_0 is the intercept of the linear fit. In this way, a first-order phase transition will exhibit a kink in the curve of the relative potential energy U_r with respect to the C_{22} percentage.

The structural features are characterized by three quantities: orientational order parameter (OOP), translational order parameter (TOP), and heterogeneity order parameter (HOP). The OOP is defined for traditional LC as the ensemble average of the second Legendre polynomial:[46]

$$S = \langle P_2(\cos\theta)\rangle \quad (3)$$

where θ is the angle between the orientation of a given C_{22} side chain and a designated global orientation. S is equal to 1 if all the vectors are ideally parallelly aligned, 0 if they all distribute randomly, around 0.5 for a nematic LC, and higher for a smectic LC.

The TOP can be used to depict the translational symmetry of crystals. A modified version for identifying the smectic structure is[16]

$$\tau = \left|\left\langle \exp\left(\frac{2\pi i z}{d}\right)\right\rangle\right| \quad (4)$$

where z is the z-component of the coordinates, and d is the interlayer spacing which takes the value that maximizes τ. Because the isotropic phase has no layered structure, d often takes the value of half the box size. The TOP value is closer to 1 for a structure with a higher translational order, and closer to 0 otherwise.

To quantify the degree of spatial heterogeneity for each type of sites, the HOP is defined by[47]

$$h = \left\langle \frac{1}{N}\sum_i \sum_j \exp\left(-\frac{r_{ij}^2}{2\sigma^2}\right)\right\rangle \quad (5)$$

where $\sigma = \left(\frac{V}{N}\right)^{1/3}$, V is the simulation box volume, N is the number of sites, and r_{ij} is the distance between sites i and j.

In addition to the above three quantities, to quantify the degree of parallelism between cationic side chains, the orientational correlation function (OCF) for C_{22} side chains is defined as[12]

$$C(r) = \langle[3(\vec{u}(\vec{r}_i)\vec{u}(\vec{r}_j))^2 - 1]\cdot\delta(\vec{r} - \vec{r}_i + \vec{r}_j)/2\rangle \quad (6)$$

where $\vec{r}_i$ is the center-of-mass (COM) position of the ith C_{22} side chain, and $\vec{u}(\vec{r}_i)$ is the corresponding unit vector pointing from the CG site A to CG site E. The probability distribution of side-chain length $P(l)$ is also calculated to reflect the tortuosity of C_{22} at different stages:

$$P(l) = \frac{1}{N}\left\langle \delta\left(l - \left|\overrightarrow{R_i}\right|\right)\right\rangle \quad (7)$$

where $|\vec{R}_i|$ is the modulus of a vector pointing from CG site A to CG site E. Moreover, the relative angular probability distribution $P_{\mathrm{ref}}(\theta)$ is introduced to quantify the degree of deviation of the angle distribution from the complete random distribution (quantified by $\sin\theta$), which is defined as

$$P_{\mathrm{ref}}(\theta) = \left\langle \frac{\delta(\vec{r} - \vec{r_i} + \vec{r_j})\delta(\arccos(|\vec{u}(\vec{r_i}) \cdot \vec{u}(\vec{r_j})|) - \theta)}{\sin\theta} \right\rangle \quad (8)$$

Both $P(l)$ and $P_{\mathrm{ref}}(\theta)$ are effective in characterizing statistically the structural features of a single C_{22} cation.

Results and discussion

Pure C_1 and C_{22}

The pure IL systems of $[C_1MIm]^+[NO_3]^-$ and $[C_{22}MIm]^+[NO_3]^-$, respectively, were simulated for comparison with the mixtures. Our simulation results indicate that pure C_1 is in the homogeneous liquid phase at T = 400 K while C_{22} is the SmB ILC under the same thermodynamic condition, consistent with the previous experimental results that $[C_1MIm]^+[NO_3]^-$ exhibits a liquid state at around T = 400 K,[48] and that the LC structures of $[C_{22}MIm]^+$ coupled with different counterions by the small angle X-ray scattering[37,38] can be identified as the SmB structure. Furthermore, by MD simulation with the united-atom model, the SmB structure has also been identified for $[C_{12}MIm]^+[PF_6]^-$, whose anion is different from and cationic side chain is shorter than $[C_{22}MIm]^+[NO_3]^-$.[49] Given by our simulations, the number densities of pure $[C_{22}MIm]^+[NO_3]^-$ and $[C_1MIm]^+[NO_3]^-$ at 400 K are 2396 mol m^{-3} and 5803 mol m^{-3}, respectively. We do not find in the literature the experimental values for these two systems, but the experimental mass density of $[C_{22}MIm]^+[NTf_2]^-$ is 1.10 g cm^{-3} at T = 383 K,[38] corresponding to a number density of 1639 mol m^{-3}, smaller than our simulated value of 2396 mol m^{-3} for $[C_{22}MIm]^+[NO_3]^-$, mainly due to the fact that $[NTf_2]^-$ is more bulky than $[NO_3]^-$, while the experimental side-chain length of 2.82 nm is exactly the same as that given by our simulation. The experimental mass density of 1,3-dimethylimidazolium methylsulfate is 1257 kg mol^{-1} at 408 K,[50] corresponding to a number density of 6043 mol m^{-3}, close to our simulated value of 5803 mol m^{-3} for $[C_1MIm]^+[NO_3]^-$.

The SmB type, also called soft crystal, is a structure between LC and crystal with hexagonal packing in the same layer and sheared between layers.[30] The representative snapshots of the equilibrated systems are shown in Fig. 2. It can be seen that pure C_1 is obviously a homogenous liquid, whereas the polar sites in C_{22} form charged layers and the side chains between layers are oriented almost identically, whose cross section exhibits hexagonal packing. The equilibrated structure of C_{22} is different from our previous MD simulation results.[12,13] In ref. 12, the C_{22} system forms a twisted and connected layered structure mainly due to the adopted *NVT* ensemble and limited simulation size of 512 ion pairs. In ref. 13, the side chains of C_{22} are globally connected but do not have a uniform normal direction, which might be a metastable state whose free energy is only slightly higher than the SmB structure obtained in this study.

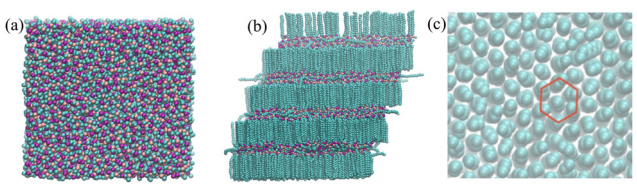

Fig. 2 Snapshots of pure C_1 (a), pure C_{22} (b), and the cross section of pure C_{22} (c).

Structures at various cation ratios

The concentration of hydrophobic side chains is varied by mixing pure C_{22} with pure C_1 at different ratios (equivalently different C_{22} percentages), and the representative snapshots of the equilibrated systems are shown in Fig. 3.

As shown in Fig. 3a, in the IL mixture with the C_{22} percentage of 5%–12.5%, C_{22} alkyl side chains well separate from each other and "float" individually in the charged "solvent" composed of anions and cation head groups. In the range from 15% to 40%, as shown in Fig. 3b, c, and d, the mixture is in the NFL phase, in which side chains tend to locally aggregate to form small bundles. The side chains in each bundle are almost perfectly parallelly aligned, but the normal directions of bundles are randomly distributed, so the entire system is still macroscopically isotropic. When the C_{22} percentage is 45%–50% (Fig. 3e), there exhibits a phase coexistence containing not only individual and bundled side chains, but also the SmB structure, which dominates when the C_{22} percentage is higher than 53.3% (Fig. 3f).

The RDFs of CG sites A–A, D–D, and E–E as well as the HOPs for A, D, and E have been calculated and are shown in Fig. 4. All three kinds of RDFs oscillate for more than 3 nm, reflecting the long electrostatic feature of the systems. The first and second peaks of the A–A and D–D RDFs increase monotonically with the C_{22} percentage, indicating that the charged groups stay closer as more C_{22} side chains join in and occupy more spaces. Correspondingly, the HOP values for A and D increase

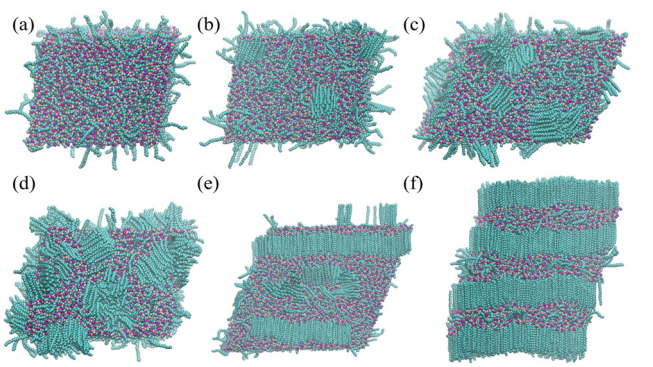

Fig. 3 Snapshots of homogeneous liquid (5%–12.5% C_{22} percentage) (a), nano-fragment liquid (15%–40%) (b), (c) and (d), coexistence phase (45%–50%) (e), and smectic B (53.3%–100%) (f).

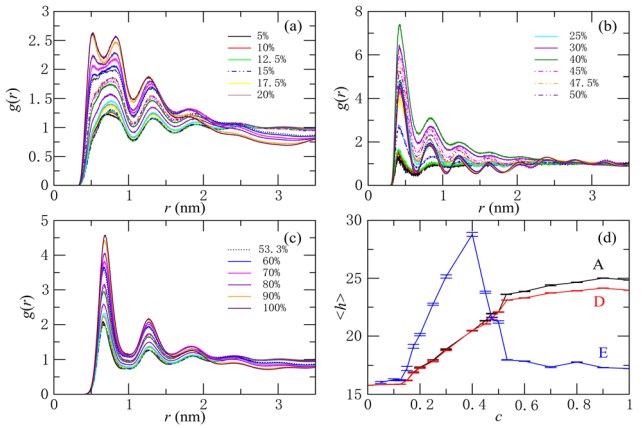

Fig. 4 Radial distribution functions for CG sites A–A (a), E–E (b), and D–D (c), as well as heterogeneity order parameters for A, D, and E (d).

monotonically with the C_{22} percentage as well. By contrast, with increasing C_{22} percentage, both the first peak of the E–E RDF and the HOP for E increase drastically starting from 15%, and then decrease after the turnover point of 40%, implying that two phase transitions occur respectively at around 15% and 40%. The first peak of the A–A RDF split into two peaks after 53.3%, indicating that many cationic head groups align parallelly in the SmB structure.

The degree of parallel alignment between side chains is quantified by the OCF, whose results are shown in Fig. 5. The OCF curves for 5%–12.5% are almost flat and remain at a very low value, which agrees with the snapshot in Fig. 3a that it is in the homogeneous liquid phase and no parallelly aligned bundles emerge. In the range from 15% to 40% (the NFL phase), the OCF takes a very high first-peak value (about 0.7 for 15% and close to 1 from 17.5% to 40%) and decays with distance approaching 0, indicating that side chains are almost perfectly aligned locally but has no long-range (global) correlation of orientation. In the range from 53.3% to 100% (the SmB phase), the first-peak value remains close to 1 within 2 nm and then decay very slowly, indicating that side chains are parallelly aligned globally with a long-range correlation of orientation.

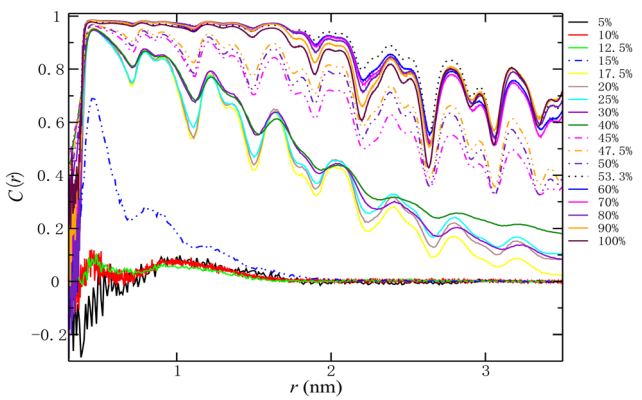

Fig. 5 Orientation correlation functions of C_{22} side chains at various C_{22} percentages.

The case for 45–50% is in between, indicating the coexistence of three phases, as will be described in detail below.

Two first-order phase transitions

The original potential energy curve shown in Fig. 6a indicates that more nonpolar C_{22} side chains make the system potential energy lower, because the attractive VDW interactions between side chains contribute negatively to the system potential energy, and better aligned side chains contribute more significantly. Meanwhile, it can hardly tell if there exist kinks or not along this curve representing latent heats, which characterize first-order phase transitions. To determine the nature of the phase behaviors of the mixture system when the number of C_{22} side chains increases, we have calculated the relative potential energy curve $U_r(c)$ defined by eqn (2), which subtracts the linear part in the isotropic phase (red dashed line in Fig. 6a) from the potential energy curve, and depicted it in Fig. 6b and c. In Fig. 6b, besides the trivial jump from 0% to 5% due to the sudden emergence of C_{22} side chains in the system, the $U_r(c)$ curve shows a kink from 15% to 17.5%, corresponding to a first-order phase transition from homogenous liquid to NFL when some of the individual C_{22} side chains aggregate to form local bundles.

If we regard $[C_{22}MIm]^+[NO_3]^-$ as the polymeric "solute" dissolved in the $[C_1MIm]^+[NO_3]^-$ "solvent", the above first-order phase transition can be theoretically understood by the Flory–Huggins theory,[51,52] which analytically quantifies the first-order phase separation of polymeric solute in solvent by

$$\Delta G = \frac{k_B T}{v_1}\left(\phi_1 \ln \phi_1 + \frac{v_1}{v_2}\phi_2 \ln \phi_2 + \chi \phi_1 \phi_2\right) \qquad (9)$$

where ΔG is the Gibbs free energy density of mixing, T is the temperature, ϕ_1 and ϕ_2 are the volume fractions of solvent and solute, respectively, v_1 and v_2 are the volumes of a single solvent and solute molecule, respectively, and x is the Huggins

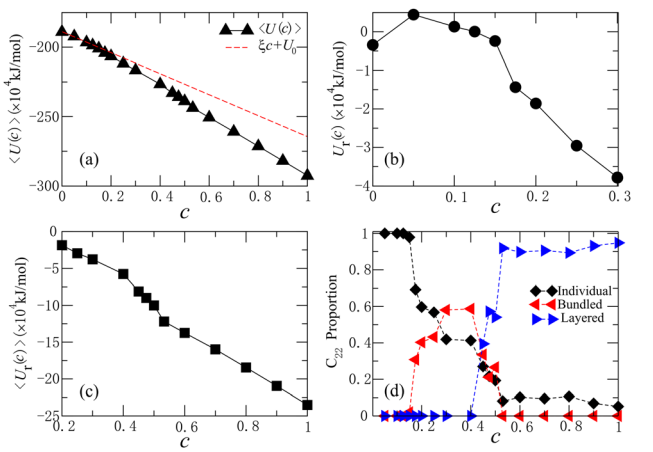

Fig. 6 (a) The potential energy curve $\langle U(c)\rangle$ (black solid line) and the linear fitting of the values at the C_{22} percentages below 15% (red dash line). (b) The relative potential energy curve $U_r(c)$ with respect to the C_{22} percentage within the range of 0%–30%. (c) $U_r(c)$ within the range of 20%–100%. (d) The proportions of C_{22} side chains in the individual, bundled, and layered states.

interaction parameter quantifying the interaction between solvent and solute molecules, which can be determined by simulation. It can be seen qualitatively that, at a fixed temperature, when C_{22} (solute) is very few, the solute can fully mix with the solvent with a uniform volume fraction, which means that C_{22} side chains are fully "dissolved" in the charged groups and stay individually; when C_{22} is beyond a certain number, the phase separation happens, leading C_{22} side chains to locally aggregate and form the NFL phase. A quantitative analysis of this first-order phase transition with the aid of the Flory–Huggins theory could be the topic of future research.

The second first-order phase transition from NFL to ILC is manifested by the sharp decrease of the slope from 40% to 53.3% in Fig. 6c. Moreover, the proportions of C_{22} side chains in three different states (individual, bundled, and layered) with respect to the C_{22} percentage are drawn in Fig. 6d. It can be seen that the proportion of individual side chains decreases steeply twice at 17.5% and 45%, respectively, which are the two phase transition points. On the other hand, the proportion of bundled side chains drastically increases at 17.5% and decreases at 45%, and keeps 0 out of this range. Correspondingly, the proportion of layered side chains suddenly increases from 0 to about half at the C_{22} percentage of 45%–50%, and remains larger than 90% after the C_{22} percentage of 53.3%. With increasing percentage of C_{22} from 53.3% to 80%, adequate effective free space allows the coexistence chemical potential to be almost constant, so the proportions of layered and individual side chains remain roughly unchanged. When the C_{22} percentage is larger than 80%, the effective free space is limited, so the configurational entropy decreases, and thus the coexistence chemical potential increases, which drives a larger proportion of individual side chains to join in the SmB layers.

The probability distributions $P(l)$ of side-chain length have been calculated and are shown in Fig. 7a. Apparently, the curves can be broken up into three different groups: from 5% to 15%, from 17.5% to 40%, and higher C_{22} percentages, corresponding to homogeneous liquid, NFL, and SmB phases. In the range of 5% to 15%, the curves reside in low probabilities and behave close to the uniform distribution, indicating that the C_{22} side chains in homogeneous liquid can freely be either straight or tortuous. When the percentage is between 17.5% and 40% in the NFL phase, $P(l)$ curves become a bit higher and a peak appears at l = 2.8 nm. For percentages larger than 53.3%, the curves peak higher at around l = 2.87 nm, indicating a straighter and nearly uniform state of the C_{22} side chains in SmB than in NFL, resulting from the stronger VDW interaction among C_{22} side chains in the layered rather than bundled structure. The $P(l)$ curves for 45%–50% behave in between NFL and SmB, reflecting the coexistence of the above three phases (see Fig. 3e). We then calculate the relative angular probability distribution $P_{\mathrm{ref}}(\theta)$ between neighboring side chains whose COM distance is less than 0.7 nm, which is roughly the position of the first valley of the E–E RDF curves (see Fig. 4b). For the ratios of 5%–15%, $P_{\mathrm{ref}}(\theta)$ is almost uniform, reflecting a random alignment of C_{22} side chains. When the C_{22} percentage is above 15%, the mutual angle θ between two neighboring side chains is mostly within 15°, which indicates a high degree of parallelism between C_{22} neighboring side chains. Obviously, the curves for 17.5%–40% and those for the 53.3%–100% group into two parts far from each other, corresponding to the NFL and SmB phases, and the $P_{\mathrm{ref}}(\theta)$ curve for the coexistence state (45%–50%) again is located in between. Therefore, the quantifications of the structural features of C_{22} side chains by $P(l)$, $P_{\mathrm{ref}}(\theta)$, and the OCF curves $C(r)$ shown in Section 3.2, support the conclusion that there are three separate phases, *i.e.*, homogeneous liquid, NFL, and SmB, with two first-order phase transitions in between when increasing the ratio of C_{22}, consistent with the relative potential energy curves shown in Fig. 6.

The dynamical properties of the IL mixtures are quantified by the diffusion coefficients shown in Fig. 8. With increasing C_{22} percentage, all diffusion coefficients for C_1 cations, C_{22} cations, and anions decrease monotonically due to stronger VDW interactions among C_{22} side chains which impairs the fluidity of all ions. The diffusion coefficient curves change their decreasing slopes twice at around 17.5% and around 50%, corresponding to the two first-order phase transitions from homogeneous liquid to NFL and from NFL to SmB, respectively.

Almost in the whole cation-ratio range, the diffusion coefficients of the three ions satisfy the relationship $D_{c_1} > D_{\mathrm{anion}} > D_{c_{22}}$, consistent with the result of $D_{c_1} > D_{\mathrm{anion}} > D_{c_{12}}$ for the IL mixture $[C_{12}/C_1MIm]^+[Tf_2N]^-$.[20] Therefore, we conclude that, similar to the $[C_{12}/C_1MIm]^+[Tf_2N]^-$ IL mixture system, no "partially-arrested glassy state" appeared in many other IL

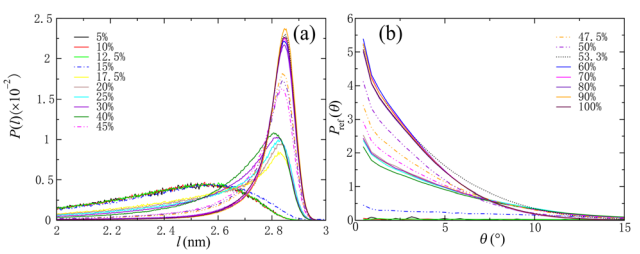

Fig. 7 (a) Probability distributions of side-chain length. (b) Probability distributions of the angle between neighboring C_{22} side chains.

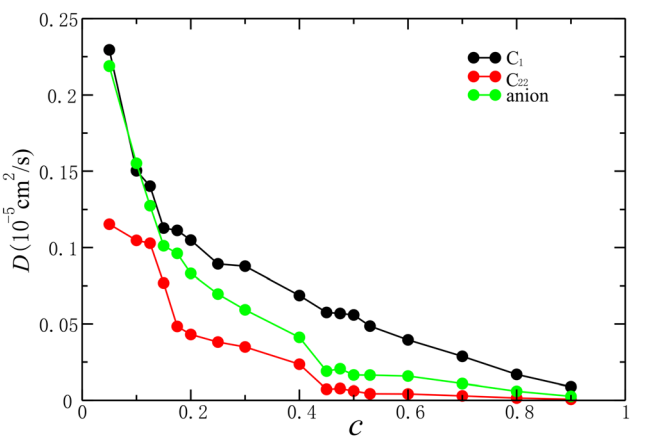

Fig. 8 Diffusion coefficients of C_1, C_{22}, and anion *versus* C_{22} percentage.

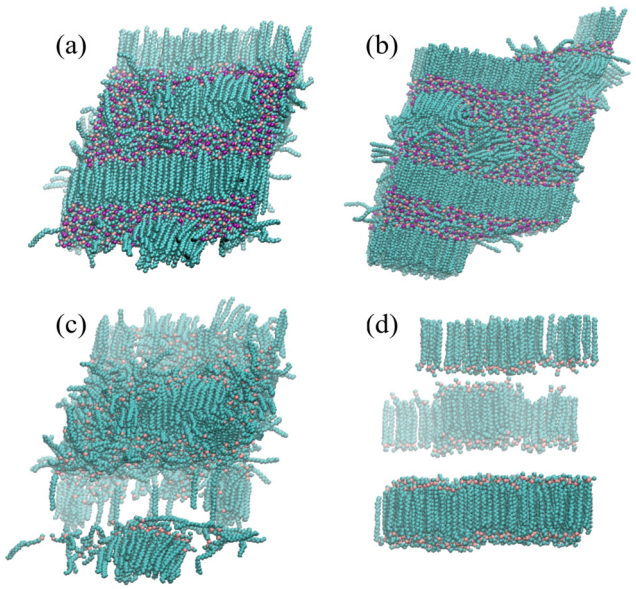

Fig. 9 Snapshots of the coexistence structures at 45% (a) and 50% (b), and the partial configurations of (a) without the SmB structure (c) and with the SmB structure only (d), respectively.

systems,[53] in which the larger cations diffuse faster than the smaller anions, is observed for $[C_{22}/C_1MIm]^+[NO_3]^-$ at T = 400 K.

Coexistence of homogeneous liquid, NFL, and SmB

The coexistence of homogeneous liquid, NFL, and SmB ILC phases is observed in our MD simulations at three simulated C_{22} percentages of 45%, 47.5% and 50%. The representative snapshots for 45% and 50% are shown in Fig. 9a and b, and that for 47.5% is already shown in Fig. 3e.

The snapshot for the coexistence structure at 45% shown in Fig. 9a can be roughly separated into two substructures containing both the homogeneous liquid and NFL phases shown in Fig. 9c as well as the SmB phase shown in Fig. 9d by identifying clusters (either bundle or layer) inside which C_{22} side chains are parallelly aligned. Layers in the SmB phase can be differentiated from bundles in the NFL phase by their comparable sizes to the simulation box. The features of homogeneous liquid, NFL, and SmB are quantified by $C(r)$, $P_{ref}(\theta)$, and $P(l)$ mentioned above, whose values for the coexistence cases are all located in between NFL and SmB (the dashed lines for 45%, 47.5%, and 50% in Fig. 5 and 7).

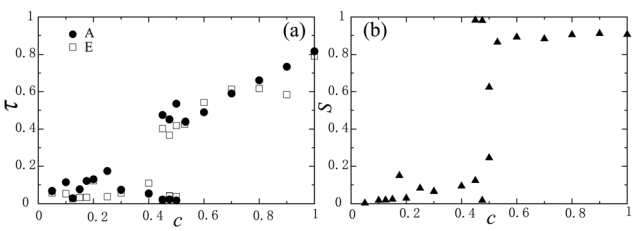

Fig. 10 (a) Translational order parameter of CG sites A and E. (b) Orientational order parameter of C_{22} side chains.

The OOP and TOP values at different percentages have been calculated and are shown in Fig. 10. It is interesting that both OOP and TOP are insensitive to the first first-order phase transition from homogeneous liquid to NFL at 15%–17.5%, because the structural difference between these two phases is local bundling of side chains, which does not cause apparent changes to global long-range orientational and translational orders. In contrast, both order parameters sharply increase to a much larger value at around 50% attributed to the large-scale structural reorganization of side chains from local bundles to global liquid crystals, again indicating that the second first-order phase transition occurs around here. Each of the two parameters has two values at a single coexistence point because it is calculated for two coexisting phases separately.

In the pure SmB structure after the second phase transition, C_1 mostly reside in the layers formed by aggregated charged sites, which weaken the correlations of C_{22} cations between charged layers. Whereas, in the coexistent structure at the C_{22} percentage around 50%, the number of C_1–D ion pairs populating between layers is the same as C_{22}–D, so the polar network formed by charged sites in the NFL strengthens the effective attraction among C_{22} side chains and eliminates the effective volume repulsion in C_{22} bundles, which prevents the system from forming a nematic-like LC, and thus leads to the transition from NFL to SmB directly. Although the nematic phase is lacking in this phase transition procedure, the formation of global alignment of side chains still results in the discontinuity in the relative potential energy curve as well.

Conclusions

In summary, our simulation results indicate that pure C_1 is a homogeneous liquid while pure C_{22} has the SmB ILC structure under the same thermodynamic conditions at T = 400 K and P = 1 bar. By increasing the C_{22} percentage, the structure of the $[C_{22}/C_1MIm]^+[NO_3]^-$ IL mixture first goes through a first-order phase transition from homogeneous liquid to NFL in the range of the C_{22} percentage from 15% to 17.5%, when the C_{22} side chains change from distributing individually to aggregating locally to form small bundles, inside which the side chains align parallelly. As the C_{22} percentage further increases, there occurs a second first-order phase transition from NFL to SmB, when the local small bundles aggregate and adjust their orientations to have their side chains align globally between charged layers with a hexagonally packed cross section. Both phase transitions are reflected by a drastic decrease in the curve of the relative potential energy, and both the global orientational and translational symmetries are broken in the second first-order phase transition. During the whole process, the curves of $P(l)$ characterizing the side-chain tortuosity, $C(r)$ characterizing the side-chain orientational correlation, and $P_{ref}(\theta)$ characterizing the degree of parallelism of neighboring side chains all exhibit three sections corresponding to the homogeneous liquid, NFL, and SmB phases, respectively. The diffusion monotonically slows down with increasing C_{22}

percentage due to the increasing effective attraction among side chains, while the slope of the slowing down changes twice around the two first-order phase transition points. Specifically, the coexistence of the homogeneous liquid, NFL, and SmB phases occurs at the C_{22} percentage ranging roughly from 45% to 50%. The flexibility of alkyl side chains allows the phase transition from NFL to SmB directly without going through the nematic phase.

Although the phase coexistence and first-order phase transitions predicted by this simulation work have not been reported by experimentalists, they are consistent with the theoretical framework of the Flory–Huggins theory[51,52] and that for the multi-phase binary system.[54] We hope that they will be observed soon in experiments. The revealed first-order phase transitions and phase coexistence is of fundamental importance to various industrial applications of ionic liquid mixtures.

Author contributions

G. S and Y. W. conceived the project and Y. W. supervised the project. J. Y. performed the simulations and data analyses. F. M. interpreted the theoretical features of the phase transitions. All authors discussed the results and wrote the manuscript.

Conflicts of interest

There are no conflicts to declare.

Acknowledgements

This work was financially supported by the National Natural Science Foundation of China (No. 11774357 and 11947302), the Italian National Research Council through the bilateral agreement CNR-NSFC 2021–2022 (NSFC grant No. 22011530390), and WIUCASQD2023009. The allocations of computer time on Tianhe-2 supercomputer and on the HPC cluster of ITP-CAS are also appreciated.

Notes and references

1 A. J. Greer, J. Jacquemin and C. Hardacre, *Molecules*, 2020, **25**, 5207.
2 H. Zhang, J. Wu, J. Zhang and J. S. He, *Macromolecules*, 2005, **38**, 8272.
3 B. C. Ranu and S. Banerjee, *Org. Lett.*, 2005, **7**, 3049.
4 N. Yamanaka, R. Kawano, W. Kubo, N. Masaki, T. Kitamura, Y. Wada, M. Watanabe and S. Yanagida, *J. Phys. Chem. B*, 2007, **111**, 4763.
5 S. Hanioka, T. Maruyama, T. Sotani, M. Teramoto, H. Matsuyama, K. Nakashima, M. Hanaki, F. Kubota and M. Goto, *J. Membr. Sci.*, 2008, **314**, 1.
6 D. Monti, E. Jónsson, M. R. Palacín and P. Johansson, *J. Power Sources*, 2014, **245**, 630.
7 M. H. Chakrabarti, F. S. Mjalli, I. M. AlNashef, M. A. Hashim, M. A. Hussain, L. Bahadori and C. T. J. Low, *Renewable Sustainable Energy Rev.*, 2014, **30**, 254.
8 A. Triolo, O. Russina, H. J. Bleif and E. Di Cola, *J. Phys. Chem. B*, 2007, **111**, 4641.
9 Y. Wang and G. A. Voth, *J. Am. Chem. Soc.*, 2005, **127**, 12192.
10 N. A. Jose, L. Canongia and A. A. H. Padua, *J. Phys. Chem. B*, 2006, **110**, 3330.
11 R. Shi and Y. Wang, *Sci. Rep.*, 2016, **6**, 19644.
12 Y. Ji, R. Shi, Y. Wang and G. Saielli, *J. Phys. Chem. B*, 2013, **117**, 1104.
13 S. Li and Y. Wang, *Sci. Rep.*, 2019, **9**, 13169.
14 G. Saielli, A. Bagno and Y. Wang, *J. Phys. Chem. B*, 2015, **119**, 3829.
15 W. Cao, B. Senthilkumar, V. Causin, V. P. Swamy, Y. Wang and G. Saielli, *Soft Matter*, 2020, **16**, 411.
16 W. Cao, Y. Wang and G. Saielli, *J. Phys. Chem. B*, 2018, **122**, 229.
17 G. Chatel, J. F. B. Pereira, V. Debbeti, H. Wang and R. D. Rogers, *Green Chem.*, 2014, **16**, 2051.
18 T. Cosby, U. Kapoor, J. K. Shah and J. Sangoro, *J. Phys. Chem. Lett.*, 2019, **10**, 6274.
19 J. K. Srivastava, R. K. Singh, R. Dharb and S. Singh, *RSC Adv.*, 2015, **5**, 86291.
20 V. Mazzilli, Y. Wang and G. Saielli, *Phys. Chem. Chem. Phys.*, 2022, **24**, 18783.
21 O. Russina, F. L. Celso, N. V. Plechkova and A. Triolo, *J. Phys. Chem. Lett.*, 2017, **8**, 1197.
22 W. M. V. Helbrun and A. Saupe, *Z. Naturforsch.*, 1958, **13**, 564.
23 W. M. V. Helbrun and A. Saupe, *Z. Naturforsch.*, 1959, **14**, 882.
24 W. M. V. Helbrun and A. Saupe, *Z. Naturforsch.*, 1960, **15**, 287.
25 W. McMillan, *Phys. Rev. A: At., Mol., Opt. Phys.*, 1971, **4**, 1238.
26 P. K. Mukherjee and J. Bhattacharya, *J. Chem. Phys.*, 2007, **126**, 024901.
27 S. Hess and P. Ilg, *Rheol. Acta*, 2005, **44**, 465.
28 L. M. Stimson and M. R. Wilsona, *J. Chem. Phys.*, 2005, **123**, 34908.
29 M. A. Bates and D. Frenkel, *J. Chem. Phys.*, 1998, **109**, 6193.
30 K. Goossens, K. Lava, C. W. Bielawski and K. Binnemans, *Chem. Rev.*, 2016, **116**, 4643.
31 F. Artzner, M. Veber, M. Clerc and A.-M. Levelut, *Liq. Cryst.*, 1997, **23**, 27.
32 A. Pană, I. Pasuk, M. Micutz and V. Cîrcu, *Cryst. Eng. Commun.*, 2016, **18**, 5066.
33 G. Saielli and K. Satoh, *Phys. Chem. Chem. Phys.*, 2019, **21**, 20327.
34 G. Saielli, T. Margola and K. Satoh, *Soft Matter*, 2017, **13**, 5204.
35 Y. Wang, W. G. Noid, P. Liu and G. A. Voth, *Phys. Chem. Chem. Phys.*, 2009, **11**, 2002.
36 Y. Wang, S. Feng and G. A. Voth, *J. Chem. Theory Comput.*, 2009, **5**, 1091.
37 D. Pontonia, M. DiMichielb and M. Deutschc, *J. Mol. Liq.*, 2020, **300**, 112280.
38 H. Weiss, J. Mars, H. Li, G. Kircher, O. Ivanova, A. Feoktystov, O. Soltwedel, M. Bier and M. Mezger, *J. Phys. Chem. B*, 2017, **121**, 620.
39 W. Cao and Y. Wang, *Crystals*, 2019, **9**, 26.
40 T. Margola, K. Satoh and G. Saielli, *Crystals*, 2018, **8**, 371.

41 M. J. Abrahama, T. Murtolad, R. Schulzb, S. A. Palla, J. C. Smithb, B. Hessa and E. Lindahla, *SoftwareX*, 2015, **1–2**, 19.
42 M. Parrinello and A. Rahman, *J. Chem. Phys.*, 2009, **130**, 074101.
43 H. J. C. Berendsen, J. P. M. Postma, W. F. van Gunsteren, A. DiNola and J. R. Haak, *J. Chem. Phys.*, 1984, **81**, 3684.
44 S. Nose, *Mol. Phys.*, 2002, **100**, 191.
45 U. Essmann, L. Perera, M. L. Berkowitz, T. Darden, H. Lee and L. G. Pedersen, *J. Chem. Phys.*, 1995, **103**, 8577.
46 M. A. Bates and G. R. Luckhurst, *Liq. Cryst.*, 1998, **24**, 229.
47 Y. Wang and G. A. Voth, *J. Phys. Chem. B*, 2006, **110**, 18601.
48 S. H. Liu and B. Zhang, *Process Saf. Environ. Prot.*, 2019, **124**, 181.
49 H. Peng, M. Kubo and H. Shiba, *Phys. Chem. Chem. Phys.*, 2018, **20**, 9796.
50 S. Aparicio, R. Alcalde, B. A. Garcia and J. M. Leal, *J. Phys. Chem. B*, 2009, **113**, 5593.
51 P. J. Flory, *J. Chem. Phys.*, 1942, **10**, 51.
52 M. L. Huggins, *J. Chem. Phys.*, 1941, **9**, 440.
53 P. E. Ramírez-Gonzalez, G. Ren, G. Saielli and Y. Wang, *J. Phys. Chem. B*, 2016, **120**, 5678.
54 J. W. Gibbs, *Trans. Conn. Acad. Arts Sci.*, 1876, **9**, 343.